

# Josephson coupling through one-dimensional ballistic channel in semiconductor-superconductor hybrid quantum point contacts

Hiroshi Irie,<sup>1,\*</sup> Yuichi Harada,<sup>1</sup> Hiroki Sugiyama,<sup>2</sup> and Tatsushi Akazaki<sup>1</sup>

<sup>1</sup>*NTT Basic Research Laboratories, NTT Corporation,  
3-1 Morinosato-Wakamiya, Atsugi 243-0198, Japan*

<sup>2</sup>*NTT Photonics Laboratories, NTT Corporation,  
3-1 Morinosato-Wakamiya, Atsugi 243-0198, Japan*

(Dated: February 29, 2024)

We study a superconducting quantum point contact made of a narrow  $\text{In}_{0.75}\text{Ga}_{0.25}\text{As}$  channel with Nb proximity electrodes. The narrow channel is formed in a gate-fitted constriction of  $\text{In-GaAs/InAlAs/InP}$  heterostructure hosting a two-dimensional electron gas. When the channel opening is varied with the gate, the Josephson critical current exhibits a discretized variation that arises from the quantization of the transverse momentum in the channel. The quantization of Josephson critical current persists down to the single-channel regime, providing an unambiguous demonstration of a semiconductor-superconductor hybrid Josephson junction involving only a single ballistic channel.

**PACS numbers:** 74.45.+c, 03.75.Lm, 73.63.Nm, 71.70.Ej

## I. INTRODUCTION

The conductance of a ballistic point contact linking two reservoirs in thermal equilibrium is quantized in multiples of the conductance quantum  $G_0 = 2e^2/h$ .<sup>1,2</sup> The origin of this phenomenon is the quantization of the transverse momentum in the narrow constriction. Strikingly,  $G_0$  is independent of the parameters characterizing the contact, and the conductance is thus solely determined by the number of modes. Another interesting feature is that the contact has a finite resistance even though no scattering is assumed at the constriction. What happens if we replace the reservoirs with superconductors? This question was answered by Beenakker and van Houten a few years after the discovery of the conductance quantization<sup>3</sup>. They theoretically analyzed a superconducting quantum point contact (SQPC) made of a smooth and impurity-free superconducting constriction, and they showed that superconducting Josephson current is carried through the Andreev bound states which are phase-coherent discrete levels formed in each quantized mode. Since the energy spectrum of these levels is insensitive to the junction properties in the short-channel limit, the Josephson critical current  $I_c$  per mode is described by the junction-independent parameters as  $I_0 = e\Delta_0/h$  ( $\Delta_0$  is the superconducting gap). Note that  $I_0$  has  $\Delta_0$  in its form in addition to the fundamental physical constants. In this respect, in contrast to the conductance quantization, the phenomenon is not universal. More theoretical work has been undertaken to take into account more realistic situations, such as a constriction longer than the superconducting coherence length, a Schottky barrier at the interface between the constriction and reservoirs, and elastic scattering in the constriction<sup>4-6</sup>. These analyses clarified that the step-like variation of  $I_c$  as a function of the mode number survives in a wide range of junction parameters, despite the fact that  $I_c$  per mode is sensitively altered by the

junction geometry and scattering process.

To prove the quantization of  $I_c$ , two types of experiments have been undertaken. The first uses a mechanically controllable break junction (MCBJ) made of two superconducting banks bridged by an atomically narrow constriction. By mechanically elongating or contracting the structure, the constriction's diameter, and hence the number of transport modes, can be tuned. A discretized change of the superconducting critical current with a step size comparable to  $e\Delta_0/h$  was observed in a Nb MCBJ<sup>7</sup>. Further study using different superconducting materials revealed that atomic valence orbitals constitute the current-carrying channels<sup>8</sup>. This finding indicates that it is difficult to manipulate either the number of transport modes or their transmission probabilities in a controlled way because these channels are extremely sensitive to the atomic configuration. Moreover, considering that even a single atom has several valence orbitals, isolating a single conducting channel is a challenging task for most metals except monovalent metals like Au<sup>9</sup>.

The second approach exploits the semiconductor-superconductor (Sm-Sc) hybrid structure. In a Sc/Sm/Sc junction, Josephson coupling is attained via Andreev reflection (AR) of quasiparticles confined in the Sm region. The transport properties of the quasiparticles, and hence the Josephson-junction (JJ) characteristics, can be controlled by means of the external electric field from a gate electrode. Quantum point contact (QPC) in a high electron mobility two-dimensional electron gas (2DEG)<sup>4,10</sup> and gate-fitted nanowires<sup>11-13</sup> have been used as Sm materials to induce quantized conducting channels. In the former case, ballistic one-dimensional (1D) channels with almost perfect transmission can be formed with comparative ease because of their long mean free path. The number of channels is electrically tunable by a gate, which offers better controllability than an MCBJ. Takayanagi *et al.*<sup>10</sup> experimentally demonstrated a 2DEG-based hybrid SQPC that utilizes

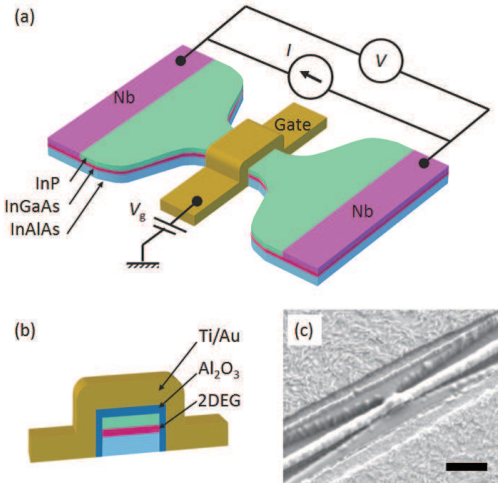


FIG. 1. (Color online) Schematic drawings of the (a) SQPC and (b) cross section of the wrap-gate QPC. (c) Scanning electron micrograph of a representative device tested. The black scale bar is 300 nm.

an InAs-based QPC with Nb proximity electrodes. They showed a stepwise change of both  $I_c$  and normal-state conductance  $G_n$  as a function of gate voltage. However, the quantization steps were vaguely visible, and the operation was limited to a few-channel regime ( $n > 4$ , where  $n$  is the number of 1D channels). Later, in a follow-up study<sup>14</sup>, it was found that  $I_c$  is excessively suppressed for  $n < 3$ , which hinders access to the single-channel operation. Other than the two reports above, there are no previous reports on this subject, and the realization of single-channel operation has been unattained so far. As for the nanowire-based hybrid SQPC, the quantized steps of  $I_c$  and  $G_n$  have not been observed in most devices using InAs nanowires<sup>12,13</sup> except for the one using a Ge/Si core/shell nanowire with Al electrodes<sup>11</sup>. In the present paper, we present a 2DEG-based hybrid SQPC that exhibits staircase variation of  $I_c$  from the multiple-channel regime down to the single-channel regime, which provides compelling evidence of the quantization of the Josephson critical current.

## II. EXPERIMENT

The device structure of the SQPC studied is illustrated in Fig. 1. Similar to the SQPCs in the previous studies<sup>10,14</sup>, it consists of a 2DEG-based QPC formed in a high-In-content InGaAs and two Nb electrodes in the vicinity of the QPC. In what follows, we describe the device structure, focusing on two major modifications to the SQPC studied previously.

Instead of the conventional finger-gate geometry, our QPC has a wrap-gate geometry, in which a narrow constriction made of an InP/In<sub>0.75</sub>Ga<sub>0.25</sub>As/InAlAs inverted-type high-electron-mobility transistor (HEMT)

structure<sup>15</sup> is wrapped with an Al<sub>2</sub>O<sub>3</sub> insulator and Ti/Au gate. The Al<sub>2</sub>O<sub>3</sub> layer was formed by the atomic layer deposition technique, which provides low interface state density, resulting in a good gate controllability. Our previous study demonstrated a well-behaved QPC operation<sup>16</sup>, i.e., conductance steps with a constant stepheight of  $G_0$ . More importantly, such clear conductance quantization is sustained even at temperatures down to 0.3 K and at zero magnetic field, where quantized steps are easily distorted due to scattering around the QPC<sup>17,18</sup>. The geometry of the QPC used here is the same as the one in Ref. 16. The width and length of the narrow constriction are 120 and 200 nm, respectively. The length of the QPC is 80 nm, which is defined by the width of the gate electrode. Electron mobility  $\mu_e$  and density  $n_s$  of the 2DEG at 1.9 K are 156,000 cm<sup>2</sup>/Vs and  $1.9 \times 10^{12}$  1/cm<sup>2</sup>, respectively. The calculated elastic mean free path  $l_e (= \hbar\mu_e/e\sqrt{2\pi n_s})$  is 3.5  $\mu$ m. Electron effective mass  $m^*$  is obtained from the temperature dependence of the Shubnikov-de Haas oscillation as  $0.043m_0$ , where  $m_0$  is the electron rest mass. Further information regarding to the wrap-gate QPC can be found in Ref. 16.

The Nb electrode, another key component of the SQPC, is fabricated by a lift-off process employing electron beam lithography. In order to achieve high AR probability, the Nb electrode has to directly touch the 2DEG, and the formation of a potential barrier at the interface should be avoided. A combination of coarse wet etching and subsequent *in situ* Ar plasma cleaning is carried out before Nb deposition. The former uses a phosphoric acid solution to selectively etch the InP layer on the InGaAs 2DEG layer. Thanks to the self-terminating process, the time required for the following *in situ* plasma cleaning can be minimized. The distance between the two Nb electrodes  $L_{ch}$  is chosen to be 300 nm. Since  $L_{ch}$  is much shorter than  $l_e$ , the SQPC is in the ballistic regime. When we discuss the superconducting properties of the SQPC,  $L_{ch}$  should also be compared with the coherence length in the 2DEG  $\xi_0 (= \hbar v_f/\pi\Delta_0)$ , where  $v_f$  and  $\Delta_0$  are the Fermi velocity and the superconducting gap). If  $\Delta_{Nb} = 1.27$  meV is used for  $\Delta_0$ , which is calculated from the critical temperature of the Nb electrode ( $T_c = 8.4$  K), we obtain  $\xi_0 = 164$  nm, giving  $L_{ch}/\xi_0 > 1$ . This indicates that the SQPC is categorized as a long junction, in which multiple Andreev levels lie in the SQPC for each transport mode<sup>19</sup>. However, as we will discuss in the next section,  $\Delta_0$  will be replaced with a smaller value when a minigap is induced in the 2DEG via the superconducting proximity effect. In this case, the SQPC is in the short-channel regime ( $L_{ch}/\xi_0 < 1$ ).

Current-voltage ( $I$ - $V$ ) characteristics of the SQPC were measured in a dilution refrigerator. Unless otherwise stated, all measurements were performed at 20 mK. A current source with a 200 k $\Omega$  load resistor was used for the bias sweep. The bias voltage  $V$  was measured by the four-terminal method using two independent contacts for each Nb electrode, which eliminated parasitic voltage drops other than that of SQPC. All the electrical lines in-

side the dilution refrigerator were twisted pairs equipped with a two-stage filter installed at the mixing chamber. The first stage comprises resistance-capacitance filters with a cutoff frequency of approximately 20 kHz. The second one consists of 2-m-long twisted pairs of constantan lines sealed tightly within folded copper tape. The latter filters out the high-frequency noise (frequency above 1 GHz), which is crucial for correctly evaluating the  $I$ - $V$  curve of a JJ<sup>20,21</sup>. In order to analyze the effects of the mode quantization,  $I$ - $V$  curves were recorded at different values of gate voltage  $V_g$ . For each  $V_g$ , 20 measurements were performed to average out the statistical variation.

### III. JOSEPHSON JUNCTION CHARACTERISTICS OF SQPC

Figure 2 shows typical  $I$ - $V$  characteristics for three representative  $V_g$  values. All  $I$ - $V$  curves show JJ characteristics with a superconducting branch at zero voltage. We define the current at which a finite voltage appears in a forward sweep as switching current  $I_{sw}$ . In a reverse sweep, the finite-voltage (resistive) state goes back to the superconducting branch at retrapping current  $I_r$ . The obtained  $I$ - $V$  curves show a hysteresis;  $I_{sw}$  is not equal to  $I_r$ , which is commonly seen in Sc/Sm or Sc/metal hybrid Josephson junctions at temperatures much below the superconducting critical temperature. The hysteresis is most likely caused by heating in the resistive state. A direct measurement of normal-metal electronic temperature in an Al/Cu JJ demonstrates that the temperature increases once the JJ switches from a superconducting state to a resistive state which results in the reduction of  $I_r$ <sup>22</sup>. Moreover, Sc/Sm hybrid JJs in general show a temperature independent  $I_r$  in the temperature range where its  $I$ - $V$  curve shows hysteresis<sup>23–25</sup>, indicating that  $I_r$  is suppressed in low-temperature limit due to the increased temperature by heating. As shown later in Fig. 4, our SQPC also shows a temperature independent  $I_r$ , supporting the idea that heating is the origin of the hysteresis in our SQPC. We note, however, that some controversial results have been reported regarding the origin of the hysteresis. A comparison between Sc/Sm/Sc junctions with and without a shunt capacitance indicates that the hysteresis is predominantly due to the underdamped nature of the JJ<sup>23</sup>. Although the intrinsic quality factor of the junction itself is very small because of the small capacitive coupling between in-plane Sc electrodes, a stray capacitance could enhance the quality factor considerably, causing the underdamped behavior<sup>20</sup>. For the underdamped JJ, we should be aware that a small fluctuation drives the JJ to switch to the resistive state below the intrinsic critical current, leading to a measured  $I_{sw}$  lower than the theoretical  $I_c$ . Nevertheless, we hereafter assume that our JJ is in the overdamped regime and that the hysteresis is caused by heating.

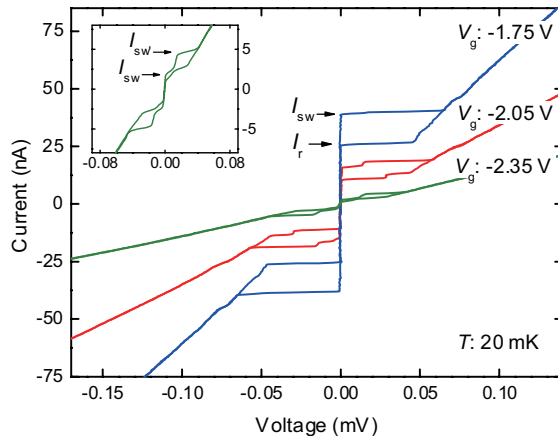


FIG. 2. (Color online)  $I$ - $V$  characteristics of the SQPC taken at three representative values of  $V_g$ . The inset shows a magnified view of the  $I$ - $V$  curve with  $V_g = -2.35$  V.

With regard to the  $V_g$  dependence of the  $I$ - $V$  curves in Fig. 2, both  $I_{sw}$  and  $I_r$  decrease with decreasing  $V_g$ , and the slope of the  $I$ - $V$  curves in the resistive state simultaneously changes with  $V_g$ . This gate controllability in terms of superconducting properties is a unique feature of the Sc/Sm hybrid JJ. We also notice that the  $I$ - $V$  curves for  $V_g = -2.05$  and  $-2.35$  V have an additional shoulder at the superconducting-to-resistive transition. A magnified view of the  $I$ - $V$  curve for  $V_g = -2.35$  V shown in the inset of Fig. 2 clearly display the shoulder at approximately 15 and 30  $\mu$ V for the forward and reverse sweep respectively. At elevated temperatures and under some  $V_g$  value, more than two shoulders appear in a single bias sweep (data not shown). These shoulders are caused by the ac Josephson effect<sup>26,27</sup> due to an unintentionally formed cavity in the measurement system. As a result, the shoulders appear at integer multiples of 15  $\mu$ V (corresponding to resonant frequency of 7.3 GHz), and these positions are the same for all three samples tested. Although this effect seems to suppress the switching current of the first transition, we take it as  $I_{sw}$  as depicted in the inset of Fig. 2. Since this suppression occurs for  $I_{sw}$  below approximately 20 nA at 20 mK, it does not affect the  $I$ - $V$  characteristics for most  $V_g$  values except near the pinch-off.

To study the effects of transport mode quantization, we show the  $V_g$  dependence of  $I_{sw}$  and differential conductance  $dI/dV$  in Figs. 3(a) and 3(b), respectively. The  $dI/dV$  is obtained by numerically differentiating an  $I$ - $V$  curve at bias voltage  $V = 0.2$  mV. The solid lines represent lines fitted using the following equations:

$$I_{\text{sw}} = I_{\text{sw}0} \sum_{n=1} T_n(V_g),$$

$$\left. \frac{dI}{dV} \right|_V^{-1} = \left[ g_0 \sum_{n=1} T_n(V_g) \right]^{-1} + R_c, \quad (1)$$

where  $I_{\text{sw}0}$  is the switching current per channel,  $g_0$  is the conductance per channel,  $R_c$  is the contact resistance at the Nb/InGaAs interface, and  $T_n(V_g)$  is the transmission probability of the  $n$ th channel. We presume here that each 1D channel contributes to the total switching current (or the conductance) by an equal amount of  $I_{\text{sw}0}$  (or  $g_0$ ) and the switching current (or the conductance) per channel is linearly dependent on the transmission probability. A saddle-point model is used to describe the potential landscape at QPC<sup>28</sup>, providing  $T_n(V_g) = \{1 + \exp[-2\pi(E_f(V_g) - E_n)/\hbar\omega_x]\}^{-1}$ , where  $E_n$  is the lowest energy of the  $n$ -th subband,  $\hbar\omega_x$  is the curvature of the saddle-point potential parallel to the current flow, and  $E_f(V_g)$  is the  $V_g$ -dependent Fermi level. For  $E_f(V_g)$ , we use the relation with a constant  $dE/dV_g$  ( $= 0.127$  eV/V)<sup>16</sup>. To calculate the fitted lines shown in the Figs. 3(a) and 3(b), we used the following set of numbers:  $(I_{\text{sw}0}, g_0, R_c, \hbar\omega_x) = (10.3$  nA,  $2.7$  G $\Omega$ ,  $230$   $\Omega$ ,  $5.9$  meV).

The main finding of the present work is the clear step-wise variation of  $I_{\text{sw}}$  with respect to  $V_g$  in Fig. 3(a), by which we unambiguously prove the Josephson coupling through the quantized 1D channels. Furthermore, the reasonable fit with  $n$ -independent step height  $I_{\text{sw}0} = 10.3$  nA (except for  $n = 1$  and  $2$ ) demonstrates both an equal contribution of each 1D channel to  $I_{\text{sw}}$  and negligible intermixing between the channels, which is consistent with existing theories. The suppressed stepheights for  $n = 1$  and  $2$  are presumably caused by the thermal activation escape because the Josephson coupling energy is comparable to the thermal energy of the bath temperature. The thermal activation escape in overdamped JJs causes the so-called phase diffusion<sup>29</sup> and results in a rounded switching in the  $I$ - $V$  curve, which is indeed seen in the inset of Fig. 2. Despite the suppression of  $I_{\text{sw}}$  for the first channel, JJ behavior with an accompanying superconducting branch is clearly observed when  $V_g$  is set such that the SQPC holds a single ballistic channel (see the inset of Fig. 2 for the  $I$ - $V$  curve).

In what follows, experimental  $I_{\text{sw}0}$  is compared with theoretical  $I_c$ . In the simplest model assuming an SQPC in the short-channel limit ( $L_{\text{ch}}/\xi_0 \ll 1$ ) with an ideal Sc/Sm interface,  $I_c$  is equal to  $e\Delta_0/\hbar$ <sup>3,4</sup>. Given the influence of a finite channel length and a Schottky barrier at the Sc/Sm interface,  $I_c$  is modified as<sup>5</sup>

$$I_c = \alpha \frac{e}{\tau}, \quad (2)$$

with

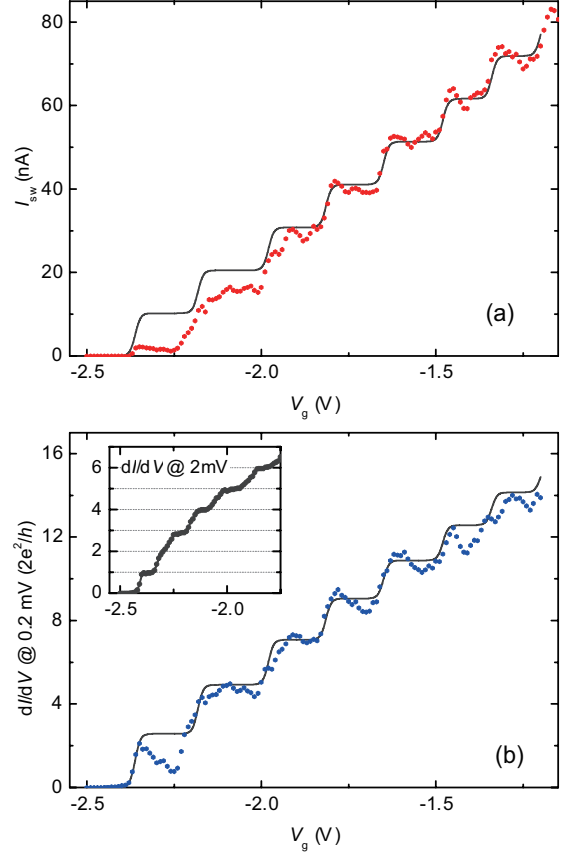


FIG. 3. (Color online) (a)  $V_g$  dependence of  $I_{\text{sw}}$ . (b)  $V_g$  dependence of  $dI/dV$  taken at  $V = 0.2$  mV. For both (a) and (b), the dots represent experimental data, while the lines are fitted curves. Refer to the main text for the details of the fitting. The inset in (b) shows  $dI/dV$  taken at  $V = 2$  mV. Note that the data in the inset were taken in a cool down cycle different from that in the main panels.

$$\tau = \frac{\hbar}{\Delta_0} + \tau_0 \left( \frac{2}{D} - 1 \right)$$

where  $\alpha$  is a coefficient determined from the Fabry-Pérot-type interference effect due to the normal reflection at the Sc/Sm interface<sup>5</sup>,  $\tau_0$  is the time of flight of a quasiparticle in 2DEG  $L_{\text{ch}}/v_f$ , and  $D$  is the tunneling probability at the Sc/Sm interface. Note that Eq. (2) is reduced to the simplest form when  $\alpha = 1$ ,  $\tau_0 \rightarrow 0$  and  $D \rightarrow 1$  are assumed. According to Ref. 3, the value of  $\alpha$  oscillates as a function of  $V_g$ , as a result of the interference condition, within a range between 1 (constructive interference) and  $D/4\pi$  (destructive interference). The value of  $D$  is determined from  $D = 1/(1 + Z^2)$ , where  $Z$  represents dimensionless barrier strength.  $Z$  can be roughly estimated from the relation  $R_N = R_{\text{Sh}}(1 + 2Z^2)$ , where  $R_N$  and  $R_{\text{Sh}}$  are the normal resistance and the



Sharvin resistance<sup>30</sup>. Using a Sc/Sm/Sc junction with a wide constriction, we obtain  $D = 0.59$  and  $Z = 0.83$  for our SQPC. Plugging  $D = 0.59$ ,  $\Delta_0 = \Delta_{\text{Nb}} = 1.27$  meV, and  $\tau_0 = 0.32$  ps (obtained with  $L_{\text{ch}} = 300$  nm and  $v_f = \frac{\hbar}{m^*} \sqrt{2\pi n_s} = 9.52 \times 10^5$  m/s) into Eq. (2) gives  $I_c$  of 125 nA for  $\alpha = 1$  and 5.9 nA for  $\alpha = D/4\pi = 0.047$ . The experimental  $I_{\text{sw}0}$  ( $= 10.3$  nA) lies between these two values, and it can be explained by assuming a  $V_g$ -independent  $\alpha$  with a value of 0.082. However, the absence of any pronounced peaks in our experimental data implies that no significant interference takes place and that  $\alpha$  should be  $\sim 1$  instead of small  $\alpha$  value. If we use  $\alpha = 1$ , the model gives  $I_c \sim 125$  nA for a single channel, which is one order of magnitude larger than the experimental  $I_{\text{sw}0}$ .

The large discrepancy can be resolved by taking into account the proximity layer at the 2DEG/Sc interface<sup>31</sup>, which has a pair potential called a minigap  $\Delta_{\text{mg}}$ . To estimate  $\Delta_{\text{mg}}$ , we fit the temperature dependence of  $I_{\text{sw}}$  using the theoretical model proposed by Kulik and Omelyanchuk (KO-2)<sup>32</sup>. In the model, the current-phase relation and critical current are described as  $I_s(\varphi) = \frac{e\Delta_0}{\hbar} \sin(\varphi/2) \tanh\left[\frac{\Delta_0 \cos(\varphi/2)}{2k_B T}\right]$  and  $I_c = \max[I_s(\varphi)]$ , respectively. Figure 4 shows the temperature dependence of the experimental  $I_{\text{sw}}$  along with two calculated  $I_c$ 's using two different  $\Delta_0$  values. Note that  $I_{\text{sw}}$  is taken at  $V_g = 0$  V, where roughly 15 channels are open, to make sure the Josephson coupling energy is larger than the thermal energy in the studied temperature range. Looking at Fig. 4, while the fit using  $\Delta_0 = \Delta_{\text{Nb}} = 1.27$  meV clearly fails to reproduce the experimental data, the best fit is obtained when  $\Delta_0 = 0.154$  meV, which we regard as  $\Delta_{\text{mg}}$ . Now,  $e\Delta_{\text{mg}}/\hbar$  gives  $I_c = 38$  nA, still larger than but of the same order as  $I_{\text{sw}0}$ . Note that we use  $e\Delta_{\text{mg}}/\hbar$  instead of Eq. (2) for calculating  $I_c$  because we do not know  $D$ , which could be drastically altered from 0.59 once the minigap is formed. This simplification overestimates  $I_c$  and could account for the remaining difference. Finally, we would like to point out that a similar  $\Delta_{\text{mg}}$  value was obtained in a system similar to our SQPC from the density of state spectra of the proximity layer formed at the Nb/In<sub>0.8</sub>Ga<sub>0.2</sub>As interface<sup>24</sup>.

In regard to the  $V_g$  dependence of  $dI/dV$  presented in Fig. 3(b), a clear stepwise change is also observed and the experimental data reasonably follow the fitted line. The striking part is that step height  $g_0$  is equal to  $2.7G_0$ , which is larger than the quantized conductance  $G_0$ . This enhancement is a consequence of the multiple ARs in the ballistic Sc/Sm/Sc junction<sup>30</sup>. In contrast to a normal QPC, in which a limited number of transport modes are available under a finite voltage bias, the Andreev-reflected quasiparticles in the SQPC carry charges through fictitious electron or hole bands without exerting additional voltage. An SQPC is an ideal platform for demonstrating this effect because the conductance is determined not by the contact resistance at the Sm/Sc interface but by the number of 1D channels. Closely looking at the data in Fig. 3(b), we notice that

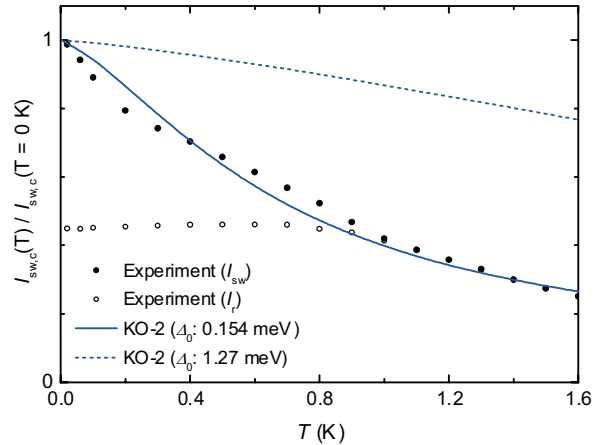


FIG. 4. (Color online) Temperature dependence of the switching current normalized by the value at 0 K. The solid and open circles are experimental data of  $I_{\text{sw}}$  and  $I_r$ , respectively. The solid and dashed lines are the curves calculated using the KO-2 model with  $\Delta_0 = 0.154$  meV and  $\Delta_0 = 1.27$  meV, respectively.

the experimental  $dI/dV$  deviates from the fitted line and exhibits a dip structure superimposed on the plateaus. This is most notable for the first plateau ( $n = 1$ ), but other plateaus ( $n = 4, 5, 6$ ) also exhibit the feature in a more subtle way. The unexpected dip is a characteristic feature in the low-bias regime. The inset of Fig. 3(b) shows  $dI/dV$ - $V_g$  at 2 mV, in which the anomalous dip structure is flattened and conventional conductance quantization in units of  $G_0$  is recovered. Since the charge transport is governed by the AR in the low-bias regime, these results indicate that the AR probability changes with  $V_g$  (or the position of the Fermi level in the QPC). The origin of this anomalous behavior is not clear, and further study is necessary to elucidate it.

#### IV. CONCLUSION

A Sc/Sm hybrid SQPC made of an In<sub>0.75</sub>Ga<sub>0.25</sub>As QPC with Nb electrodes is examined. The quantization of  $I_c$  is demonstrated by the staircase variation of  $I_{\text{sw}}$ . The staircase variation persists down to the single-channel regime, providing the first unambiguous demonstration of a Josephson junction with a single ballistic channel using Sc/Sm hybrid SQPCs. Although this quantized critical current has already been reported, the results presented in this paper prove it in a much clearer fashion. Beyond the experimental proof of quantized  $I_c$ , the realization of SQPC, especially single channel operation, opens up interesting possibilities for the application in quantum information processing. A pair of Andreev levels in a single channel SQPC forms a doublet state that can be utilized as a quantum bit<sup>33</sup>. Recently,

a spectroscopy analysis of the Andreev levels in an Al-based MCBJ was performed, and its phase-dependent energy levels were successfully demonstrated<sup>27</sup>. The studied SQPC allows us to precisely control the channel number, which is an advantage in realizing the Andreev level qubits.

## ACKNOWLEDGMENTS

This work was supported by the "Topological Quantum Phenomena" (No. 22103002) Grant-in Aid for Scientific Research on Innovative Areas from the Ministry of Education, Culture, Sports, Science and Technology (MEXT) of Japan.

- 
- \* irie.hiroshi@lab.ntt.co.jp
- <sup>1</sup> B. J. van Wees, H. van Houten, C. W. J. Beenakker, J. G. Williamson, L. P. Kouwenhoven, D. van der Marel, and C. T. Foxon, *Phys. Rev. Lett.* **60**, 848 (1988).
  - <sup>2</sup> D. A. Wharam, T. J. Thornton, R. Newbury, M. Pepper, H. Ahmed, J. E. F. Frost, D. G. Hasko, D. C. Peacock, D. A. Ritchie, and G. A. C. Jones, *J. Phys. C*: **21**, L209 (1988).
  - <sup>3</sup> C. W. J. Beenakker and H. van Houten, *Phys. Rev. Lett.* **66**, 3056 (1991).
  - <sup>4</sup> A. Furusaki, H. Takayanagi, and M. Tsukada, *Phys. Rev. Lett.* **67**, 132 (1991); *Phys. Rev. B* **45**, 10563 (1992).
  - <sup>5</sup> N. Shchelkachev, *JETP Lett.* **71**, 504 (2000).
  - <sup>6</sup> N. M. Chitchev, G. B. Lesovik, and G. Blatter, *Phys. Rev. B* **62**, 3559 (2000).
  - <sup>7</sup> C. J. Muller, J. M. van Ruitenbeek, and L. J. de Jongh, *Phys. Rev. Lett.* **69**, 140 (1992).
  - <sup>8</sup> E. Scheer, N. Agraït, J. Cuevas, A. Yeyati, B. Ludoph, A. Martin-Rodero, G. Bollinger, J. van Ruitenbeek, and C. Urbina, *Nature (London)* **394**, 154 (1998).
  - <sup>9</sup> E. Scheer, W. Belzig, Y. Naveh, M. H. Devoret, D. Esteve, and C. Urbina, *Phys. Rev. Lett.* **86**, 284 (2001).
  - <sup>10</sup> H. Takayanagi, T. Akazaki, and J. Nitta, *Phys. Rev. Lett.* **75**, 3533 (1995).
  - <sup>11</sup> J. Xiang, A. Vidan, M. Tinkham, R. M. Westervelt, and C. M. Lieber, *Nat. Nanotechnol.* **1**, 208 (2006).
  - <sup>12</sup> Y. Doh, J. van Dam, A. Roest, E. Bakkers, L. Kouwenhoven, and S. De Franceschi, *Science* **309**, 272 (2005).
  - <sup>13</sup> T. Nishio, T. Kozakai, S. Amaha, M. Larsson, H. A. Nilsson, H. Q. Xu, G. Zhang, K. Tateno, H. Takayanagi, and K. Ishibashi, *Nanotechnology* **22**, 445701 (2011).
  - <sup>14</sup> T. Bauch, E. Hürfeld, V. M. Krasnov, P. Delsing, H. Takayanagi, and T. Akazaki, *Phys. Rev. B* **71**, 174502 (2005).
  - <sup>15</sup> The actual layer structure is, from the bottom to the surface, an undoped  $\text{In}_{0.52}\text{Al}_{0.48}\text{As}$  buffer (200 nm), a  $\text{Si } 4 \times 10^{18} \text{ cm}^{-3}$  doped layer (6 nm), an undoped  $\text{In}_{0.52}\text{Al}_{0.48}\text{As}$  spacer (10 nm), a composite 2DEG layer consisting of  $\text{In}_{0.53}\text{Ga}_{0.47}\text{As}/\text{In}_{0.75}\text{Ga}_{0.25}\text{As}/\text{In}_{0.53}\text{Ga}_{0.47}\text{As}$  (2.5/8/5 nm), an undoped  $\text{In}_{0.52}\text{Al}_{0.48}\text{As}$  layer (3 nm), an undoped  $\text{InP}$  surface layer (5 nm).
  - <sup>16</sup> H. Irie, Y. Harada, H. Sugiyama, and T. Akazaki, *Appl. Phys. Express* **5**, 024001 (2012).
  - <sup>17</sup> T. Schäpers, V. A. Guzenko, and H. Hardtdegen, *Appl. Phys. Lett.* **90**, 122107 (2007).
  - <sup>18</sup> P. Ramvall, N. Carlsson, I. Maximov, P. Omling, L. Samuelson, W. Seifert, Q. Wang, and S. Lourdudoss, *Appl. Phys. Lett.* **71**, 918 (1997).
  - <sup>19</sup> T. Schäpers, *Superconductor/Semiconductor Junctions* (Springer, 2001).
  - <sup>20</sup> P. Jarillo-Herrero, J. van Dam, and L. Kouwenhoven, *Nature (London)* **439**, 953 (2006).
  - <sup>21</sup> L. C. Mur, C. J. P. M. Harmans, J. E. Mooij, J. F. Carlin, A. Rudra, and M. Ilegems, *Phys. Rev. B* **54**, R2327 (1996).
  - <sup>22</sup> H. Courtois, M. Meschke, J. T. Peltonen, and J. P. Pekola, *Phys. Rev. Lett.* **101**, 067002 (2008).
  - <sup>23</sup> V. M. Krasnov, T. Bauch, S. Intiso, E. Hürfeld, T. Akazaki, H. Takayanagi, and P. Delsing, *Phys. Rev. Lett.* **95**, 157002 (2005).
  - <sup>24</sup> F. Deon, V. Pellegrini, F. Giazotto, G. Biasiol, L. Sorba, and F. Beltram, *Phys. Rev. B* **84**, 100506 (2011).
  - <sup>25</sup> T. Schäpers, A. Kaluza, K. Neurohr, J. Malindretos, G. Creclius, A. vanderHart, H. Hardtdegen, and H. Luth, *Appl. Phys. Lett.* **71**, 3575 (1997).
  - <sup>26</sup> M. Levinsen, *Appl. Phys. Lett.* **24**, 247 (1974).
  - <sup>27</sup> L. Bretheau, Ç. Ö. Girit, H. Pothier, D. Esteve, and C. Urbina, *Nature (London)* **499**, 312 (2013).
  - <sup>28</sup> M. Büttiker, *Phys. Rev. B* **41**, 7906 (1990).
  - <sup>29</sup> V. Mel'nikov, *Physics Reports* **209**, 1 (1991).
  - <sup>30</sup> M. Octavio, M. Tinkham, G. E. Blonder, and T. M. Klapwijk, *Phys. Rev. B* **27**, 6739 (1983).
  - <sup>31</sup> B. A. Aminov, A. A. Golubov, and M. Y. Kupriyanov, *Phys. Rev. B* **53**, 365 (1996).
  - <sup>32</sup> I. O. Kulik and A. N. Omel'yanchuk, *Sov. J. Low. Temp. Phys.* **3**, 459 (1977); **4**, 142 (1978).
  - <sup>33</sup> A. Zazunov, V. S. Shumeiko, E. N. Bratus', J. Lantz, and G. Wendin, *Phys. Rev. Lett.* **90**, 087003 (2003).